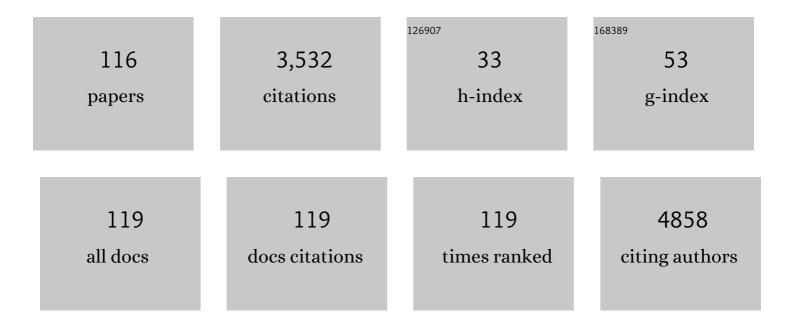
## Wojciech Lisowski

List of Publications by Year in descending order

Source: https://exaly.com/author-pdf/1053288/publications.pdf Version: 2024-02-01



#	Article	IF	CITATIONS
1	Ti/TiO2 nanotubes sensitized PbS quantum dots as photoelectrodes applied for decomposition of anticancer drugs under simulated solar energy. Journal of Hazardous Materials, 2022, 421, 126751.	12.4	16
2	The influence of ILs on TiO2 microspheres activity towards 5-FU removal under artificial sunlight irradiation. Applied Surface Science, 2022, 573, 151431.	6.1	4
3	Indium(II) Chloride as a Precursor in the Synthesis of Ternary (Ag–In–S) and Quaternary (Ag–In–Zn–S) Nanocrystals. Chemistry of Materials, 2022, 34, 809-825.	6.7	7
4	Solar-driven photoelectrocatalytic degradation of anticancer drugs using TiO <sub>2</sub> nanotubes decorated with SnS quantum dots. Dalton Transactions, 2022, 51, 5962-5976.	3.3	2
5	Lead-free bismuth-based perovskites coupled with g–C3N4: A machine learning based novel approach for visible light induced degradation of pollutants. Applied Surface Science, 2022, 588, 152921.	6.1	13
6	A novel (Ti/Ce)UiO-X MOFs@TiO2 heterojunction for enhanced photocatalytic performance: Boosting via Ce4+/Ce3+ and Ti4+/Ti3+ redox mediators. Applied Catalysis B: Environmental, 2022, 310, 121349.	20.2	28
7	Diazonium-Based Covalent Molecular Wiring of Single-Layer Graphene Leads to Enhanced Unidirectional Photocurrent Generation through the p-doping Effect. Chemistry of Materials, 2022, 34, 3744-3758.	6.7	2
8	Ni(OH) <sub>2</sub> -Type Nanoparticles Derived from Ni Salen Polymers: Structural Design toward Functional Materials for Improved Electrocatalytic Performance. ACS Applied Materials & Interfaces, 2022, 14, 33768-33786.	8.0	3
9	Remarkable visible-light induced hydrogen generation with ZnIn2S4 microspheres/CuInS2 quantum dots photocatalytic system. International Journal of Hydrogen Energy, 2021, 46, 486-498.	7.1	44
10	Electrochemical sensor for selective tyramine determination, amplified by a molecularly imprinted polymer film. Bioelectrochemistry, 2021, 138, 107695.	4.6	26
11	Effect of synthesis method parameters on properties and photoelectrocatalytic activity under solar irradiation of TiO2 nanotubes decorated with CdS quantum dots. Journal of Environmental Chemical Engineering, 2021, 9, 104816.	6.7	14
12	Stannates, titanates and tantalates modified with carbon and graphene quantum dots for enhancement of visible-light photocatalytic activity. Applied Surface Science, 2021, 541, 148425.	6.1	16
13	Selective Oxidation of 5â€Hydroxymethylfurfural to 2,5â€Diformylfuran by Visible Lightâ€Driven Photocatalysis over In Situ Substrateâ€Sensitized Titania. ChemSusChem, 2021, 14, 1351-1362.	6.8	53
14	Insights into the Intrinsic Creation of Heterojunction-Based Ordered TiO <sub>2</sub> Nanotubes Obtained from the One-Step Anodic Oxidation of Titanium Alloys. Journal of Physical Chemistry C, 2021, 125, 7097-7108.	3.1	6
15	Improvement of Ni/Al <sub>2</sub> O <sub>3</sub> Catalysts for Low-Temperature CO <sub>2</sub> Methanation by Vanadium and Calcium Oxide Addition. Industrial & Engineering Chemistry Research, 2021, 60, 6554-6564.	3.7	20
16	Self-Reporting Molecularly Imprinted Polymer with Covalently Immobilized Ferrocene Redox Probe for Selective Electrochemical Sensing of P-Synephrine. ECS Meeting Abstracts, 2021, MA2021-01, 1368-1368.	0.0	0
17	Towards Computer-Aided Graphene Covered TiO2-Cu/(CuxOy) Composite Design for the Purpose of Photoinduced Hydrogen Evolution. Catalysts, 2021, 11, 698.	3.5	3
18	Nanostructured Molecular Imprinted Polymers for Chemosensing of Hormone Proteins. ECS Meeting Abstracts, 2021, MA2021-01, 1690-1690.	0.0	1

#	Article	IF	CITATIONS
19	Visible-light-driven lanthanide-organic-frameworks modified TiO2 photocatalysts utilizing up-conversion effect. Applied Catalysis B: Environmental, 2021, 291, 120056.	20.2	35
20	Novel two-step synthesis method of thin film heterojunction of BiOBr/Bi2WO6 with improved visible-light-driven photocatalytic activity. Applied Surface Science, 2021, 569, 151082.	6.1	24
21	Titania/chitosan–lignin nanocomposite as an efficient photocatalyst for the selective oxidation of benzyl alcohol under UV and visible light. RSC Advances, 2021, 11, 34996-35010.	3.6	7
22	Selective Impedimetric Chemosensing of Carcinogenic Heterocyclic Aromatic Amine in Pork by dsDNA-Mimicking Molecularly Imprinted Polymer Film-Coated Electrodes. Journal of Agricultural and Food Chemistry, 2021, 69, 14689-14698.	5.2	7
23	Materials characterization of TiO <sub>2</sub> nanotubes decorated by Au nanoparticles for photoelectrochemical applications. RSC Advances, 2021, 11, 38727-38738.	3.6	11
24	Hexagonally Packed Macroporous Molecularly Imprinted Polymers for Chemosensing of Follicle-Stimulating Hormone Protein. ACS Sensors, 2020, 5, 118-126.	7.8	23
25	Fabrication of ILs-Assisted AgTaO3 Nanoparticles for the Water Splitting Reaction: The Effect of ILs on Morphology and Photoactivity. Materials, 2020, 13, 4055.	2.9	1
26	Integrated Experimental and Theoretical Approach for Efficient Design and Synthesis of Gold-Based Double Halide Perovskites. Journal of Physical Chemistry C, 2020, 124, 26769-26779.	3.1	10
27	Noble Metal Nanoparticles in Pectin Matrix. Preparation, Film Formation, Property Analysis, and Application in Electrocatalysis. ACS Omega, 2020, 5, 23909-23918.	3.5	9
28	Theoretical and Experimental Studies on the Visible Light Activity of TiO2 Modified with Halide-Based Ionic Liquids. Catalysts, 2020, 10, 371.	3.5	6
29	Experimental and DFT insights into an eco-friendly photocatalytic system toward environmental remediation and hydrogen generation based on AgInS2 quantum dots embedded on Bi2WO6. Applied Surface Science, 2020, 525, 146596.	6.1	32
30	Synergy between AgInS2 quantum dots and ZnO nanopyramids for photocatalytic hydrogen evolution and phenol degradation. Journal of Hazardous Materials, 2020, 398, 123250.	12.4	22
31	Urchin-like TiO2 structures decorated with lanthanide-doped Bi2S3 quantum dots to boost hydrogen photogeneration performance. Applied Catalysis B: Environmental, 2020, 272, 118962.	20.2	68
32	Plasma Nitriding of TiO <sub>2</sub> Nanotubes: N-Doping in Situ Investigations Using XPS. ACS Omega, 2020, 5, 8647-8658.	3.5	41
33	Ordered TiO <sub>2</sub> Nanotubes with Improved Photoactivity through Self-organizing Anodization with the Addition of an Ionic Liquid: Effects of the Preparation Conditions. ACS Sustainable Chemistry and Engineering, 2019, 7, 15585-15596.	6.7	8
34	Electrochemically initiated co-polymerization of monomers of different oxidation potentials for molecular imprinting of electroactive analyte. Sensors and Actuators B: Chemical, 2019, 298, 126884.	7.8	16
35	Fabrication of Durable Ordered Ta2O5 Nanotube Arrays Decorated with Bi2S3 Quantum Dots. Nanomaterials, 2019, 9, 1347.	4.1	9
36	The effect of imidazolium ionic liquid on the morphology of Pt nanoparticles deposited on the surface of SrTiO3 and photoactivity of Pt–SrTiO3 composite in the H2 generation reaction. International Journal of Hydrogen Energy, 2019, 44, 26308-26321.	7.1	18

#	Article	IF	CITATIONS
37	Shape-controllable synthesis of GdVO <sub>4</sub> photocatalysts and their tunable properties in photocatalytic hydrogen generation. Dalton Transactions, 2019, 48, 1662-1671.	3.3	20
38	Impact of Tetrazolium Ionic Liquid Thermal Decomposition in Solvothermal Reaction on the Remarkable Photocatalytic Properties of TiO2 Particles. Nanomaterials, 2019, 9, 744.	4.1	5
39	Promoting bioanalytical concepts in genetics: A TATA box molecularly imprinted polymer as a small isolated fragment of the DNA damage repairing system. Materials Science and Engineering C, 2019, 100, 1-10.	7.3	7
40	Facile Fabrication of Surface-Imprinted Macroporous Films for Chemosensing of Human Chorionic Gonadotropin Hormone. ACS Applied Materials & Interfaces, 2019, 11, 9265-9276.	8.0	33
41	Gold Nanoparticles Functionalized with Fully Conjugated Fullerene C <sub>60</sub> Derivatives as a Material with Exceptional Capability of Absorbing Electrons. Journal of Physical Chemistry C, 2019, 123, 6229-6240.	3.1	8
42	Optical and photocatalytic properties of rare earth metal-modified ZnO quantum dots. Applied Surface Science, 2019, 464, 651-663.	6.1	64
43	A new simple approach to prepare rare-earth metals-modified TiO2 nanotube arrays photoactive under visible light: Surface properties and mechanism investigation. Results in Physics, 2019, 12, 412-423.	4.1	30
44	Mono- and bimetallic nanoparticles decorated KTaO3 photocatalysts with improved Vis and UV–Vis light activity. Applied Surface Science, 2018, 441, 993-1011.	6.1	26
45	Surface characterization of low-temperature grown yttrium oxide. Applied Surface Science, 2018, 437, 347-356.	6.1	10
46	Dependence between Ionic Liquid Structure and Mechanism of Visible-Light-Induced Activity of TiO <sub>2</sub> Obtained by Ionic-Liquid-Assisted Solvothermal Synthesis. ACS Sustainable Chemistry and Engineering, 2018, 6, 3927-3937.	6.7	21
47	Visible light photocatalysis employing TiO2/SrTiO3-BiOI composites: Surface properties and photoexcitation mechanism. Molecular Catalysis, 2018, 452, 154-166.	2.0	18
48	Rare earth ions doped K2Ta2O6 photocatalysts with enhanced UV–vis light activity. Applied Catalysis B: Environmental, 2018, 224, 451-468.	20.2	46
49	Synthesis and application of a "plastic antibody―in electrochemical microfluidic platform for oxytocin determination. Biosensors and Bioelectronics, 2018, 100, 251-258.	10.1	39
50	Studies on novel BiyXz-TiO2/SrTiO3 composites: Surface properties and visible light-driven photoactivity. Applied Surface Science, 2018, 435, 1174-1186.	6.1	16
51	Facile Formation of Self-Organized TiO <sub>2</sub> Nanotubes in Electrolyte Containing Ionic Liquid-Ethylammonium Nitrate and Their Remarkable Photocatalytic Properties. ACS Sustainable Chemistry and Engineering, 2018, 6, 14510-14522.	6.7	9
52	TiO <sub>2</sub> and NaTaO <sub>3</sub> Decorated by Trimetallic Au/Pd/Pt Core–Shell Nanoparticles as Efficient Photocatalysts: Experimental and Computational Studies. ACS Sustainable Chemistry and Engineering, 2018, 6, 16665-16682.	6.7	38
53	Fabrication and photoactivity of ionic liquid–TiO <sub>2</sub> structures for efficient visible-light-induced photocatalytic decomposition of organic pollutants in aqueous phase. Beilstein Journal of Nanotechnology, 2018, 9, 580-590.	2.8	17
54	Monometallic nanoparticles decorated and rare earth ions doped KTaO3/K2Ta2O6 photocatalysts with enhanced pollutant decomposition and improved H2 generation. Journal of Catalysis, 2018, 364, 371-381.	6.2	29

#	Article	IF	CITATIONS
55	Highly Active TiO2 Microspheres Formation in the Presence of Ethylammonium Nitrate Ionic Liquid. Catalysts, 2018, 8, 279.	3.5	10
56	Shape-dependent enhanced photocatalytic effect under visible light of Ag3PO4 particles. Journal of Photochemistry and Photobiology A: Chemistry, 2018, 367, 240-252.	3.9	33
57	Oligonucleotide Determination via Peptide Nucleic Acid Macromolecular Imprinting in an Electropolymerized CG-Rich Artificial Oligomer Analogue. ACS Applied Materials & Interfaces, 2018, 10, 27562-27569.	8.0	25
58	Electrochemically Obtained TiO2/CuxOy Nanotube Arrays Presenting a Photocatalytic Response in Processes of Pollutants Degradation and Bacteria Inactivation in Aqueous Phase. Catalysts, 2018, 8, 237.	3.5	16
59	Influence of the preparation method on the photocatalytic activity of Nd-modified TiO <sub>2</sub> . Beilstein Journal of Nanotechnology, 2018, 9, 447-459.	2.8	34
60	TiO2CoxOy composite nanotube arrays via one step electrochemical anodization for visible light–induced photocatalytic reaction. Surfaces and Interfaces, 2018, 12, 179-189.	3.0	10
61	Design and Fabrication of TiO <sub>2</sub> /Lignocellulosic Carbon Materials: Relevance of Lowâ€ŧemperature Sonocrystallization to Photocatalysts Performance. ChemCatChem, 2018, 10, 3469-3480.	3.7	35
62	Programmed Transfer of Sequence Information into a Molecularly Imprinted Polymer for Hexakis(2,2′-bithien-5-yl) DNA Analogue Formation toward Single-Nucleotide-Polymorphism Detection. ACS Applied Materials & Interfaces, 2017, 9, 3948-3958.	8.0	25
63	Photocatalytically Active TiO <sub>2</sub> /Ag <sub>2</sub> O Nanotube Arrays Interlaced with Silver Nanoparticles Obtained from the One-Step Anodic Oxidation of Ti–Ag Alloys. ACS Catalysis, 2017, 7, 2753-2764.	11.2	76
64	Hierarchical templating in deposition of semi-covalently imprinted inverse opal polythiophene film for femtomolar determination of human serum albumin. Biosensors and Bioelectronics, 2017, 94, 155-161.	10.1	47
65	Novel decahedral TiO 2 photocatalysts modified with Ru or Rh NPs: Insight into the mechanism. Molecular Catalysis, 2017, 434, 154-166.	2.0	19
66	Facile Gram-Scale Synthesis of the First n-Type CuFeS2 Nanocrystals for Thermoelectric Applications. European Journal of Inorganic Chemistry, 2017, 2017, 3150-3153.	2.0	17
67	Dual Functionality of TiO <sub>2</sub> /Biochar Hybrid Materials: Photocatalytic Phenol Degradation in the Liquid Phase and Selective Oxidation of Methanol in the Gas Phase. ACS Sustainable Chemistry and Engineering, 2017, 5, 6274-6287.	6.7	130
68	Use of XPS to clarify the Hall coefficient sign variation in thin niobium layers buried in silicon. Applied Surface Science, 2017, 399, 32-40.	6.1	11
69	Enhanced photocatalytic properties of lanthanide-TiO2 nanotubes: An experimental and theoretical study. Applied Catalysis B: Environmental, 2017, 205, 376-385.	20.2	87
70	Luminophores of tunable colors from ternary Ag–In–S and quaternary Ag–In–Zn–S nanocrystals covering the visible to near-infrared spectral range. Physical Chemistry Chemical Physics, 2017, 19, 1217-1228.	2.8	29
71	The effect of metals content on the photocatalytic activity of TiO2 modified by Pt/Au bimetallic nanoparticles prepared by sol-gel method. Molecular Catalysis, 2017, 442, 154-163.	2.0	43
72	Preparation and photocatalytic properties of BaZrO 3 and SrZrO 3 modified with Cu 2 O/Bi 2 O 3 quantum dots. Solid State Sciences, 2017, 74, 13-23.	3.2	29

5

#	Article	IF	CITATIONS
73	Highly Visible-Light-Photoactive Heterojunction Based on TiO <sub>2</sub> Nanotubes Decorated by Pt Nanoparticles and Bi <sub>2</sub> S <sub>3</sub> Quantum Dots. Journal of Physical Chemistry C, 2017, 121, 17215-17225.	3.1	30
74	Visibleâ€Light Photocatalytic Activity of Ionic Liquid TiO <sub>2</sub> Spheres: Effect of the Ionic Liquid's Anion Structure. ChemCatChem, 2017, 9, 4377-4388.	3.7	21
75	Preparation and photocatalytic activity of Nd-modified TiO2 photocatalysts: Insight into the excitation mechanism under visible light. Journal of Catalysis, 2017, 353, 211-222.	6.2	43
76	The effects of bifunctional linker and reflux time on the surface properties and photocatalytic activity of CdTe quantum dots decorated KTaO3 composite photocatalysts. Applied Catalysis B: Environmental, 2017, 203, 452-464.	20.2	50
77	Effect of irradiation intensity and initial pollutant concentration on gas phase photocatalytic activity of TiO 2 nanotube arrays. Catalysis Today, 2017, 284, 19-26.	4.4	51
78	Gold Catalysts on Y-Doped Ceria Supports for Complete Benzene Oxidation. Catalysts, 2016, 6, 99.	3.5	11
79	Photocatalytic activity of nitrogen doped TiO2 nanotubes prepared by anodic oxidation: The effect of applied voltage, anodization time and amount of nitrogen dopant. Applied Catalysis B: Environmental, 2016, 196, 77-88.	20.2	110
80	The effect of gold shape and size on the properties and visible light-induced photoactivity of Au-TiO2. Applied Catalysis B: Environmental, 2016, 196, 27-40.	20.2	83
81	Non-injection synthesis of monodisperse Cu–Fe–S nanocrystals and their size dependent properties. Physical Chemistry Chemical Physics, 2016, 18, 15091-15101.	2.8	23
82	Cu–Fe–S Nanocrystals Exhibiting Tunable Localized Surface Plasmon Resonance in the Visible to NIR Spectral Ranges. Inorganic Chemistry, 2016, 55, 6660-6669.	4.0	39
83	Early diagnosis of fungal infections using piezomicrogravimetric and electric chemosensors based on polymers molecularly imprinted with d-arabitol. Biosensors and Bioelectronics, 2016, 79, 627-635.	10.1	40
84	Synthesis and characterization of porous carbon–MoS <sub>2</sub> nanohybrid materials: electrocatalytic performance towards selected biomolecules. Journal of Materials Chemistry B, 2016, 4, 1448-1457.	5.8	23
85	The ILs-assisted solvothermal synthesis of TiO2 spheres: The effect of ionic liquids on morphology and photoactivity of TiO2. Applied Catalysis B: Environmental, 2016, 184, 223-237.	20.2	58
86	Surface studies of praseodymium by electron spectroscopies. Applied Surface Science, 2016, 388, 691-695.	6.1	2
87	An electropolymerized molecularly imprinted polymer for selective carnosine sensing with impedimetric capacity. Journal of Materials Chemistry B, 2016, 4, 1156-1165.	5.8	21
88	Decoration of MoS2 Nanopetal Stacks with Positively Charged Gold Nanoparticles for Synergistic Electrocatalytic Oxidation of Biologically Relevant Compounds. Electrochimica Acta, 2015, 182, 659-667.	5.2	8
89	Visible light activity of rare earth metal doped (Er3+, Yb3+ or Er3+/Yb3+) titania photocatalysts. Applied Catalysis B: Environmental, 2015, 163, 40-49.	20.2	295
90	Lanthanide co-doped TiO2: The effect of metal type and amount on surface properties and photocatalytic activity. Applied Surface Science, 2014, 307, 333-345.	6.1	139

#	Article	IF	CITATIONS
91	Electrocatalytic Synergy on Nanoparticulate Films Prepared from Oppositely Charged Pt and Au Nanoparticles. ChemElectroChem, 2014, 1, 1023-1026.	3.4	6
92	Ligand exchange in quaternary alloyed nanocrystals – a spectroscopic study. Physical Chemistry Chemical Physics, 2014, 16, 23082-23088.	2.8	38
93	Visible light photoactivity of TiO2 loaded with monometallic (Au or Pt) and bimetallic (Au/Pt) nanoparticles. Applied Surface Science, 2014, 317, 1131-1142.	6.1	61
94	XPS method as a useful tool for studies of quantum well epitaxial materials: Chemical composition and thermal stability of InGaN/GaN multilayers. Journal of Alloys and Compounds, 2014, 597, 181-187.	5.5	5
95	Molecularly imprinted polymer of bis(2,2′-bithienyl)methanes for selective determination of adrenaline. Bioelectrochemistry, 2013, 93, 37-45.	4.6	44
96	Studies of the hot-pressed TiN material by electron spectroscopies. Journal of Alloys and Compounds, 2013, 546, 280-285.	5.5	14
97	Hydrophilic polycarbonate chips for generation of oil-in-water (O/W) and water-in-oil-in-water (W/O/W) emulsions. Microfluidics and Nanofluidics, 2013, 14, 597-604.	2.2	12
98	Hydrophilic polycarbonate chips for generation of oil-in-water (O/W) and water-in-oil-in-water (W/O/W) emulsions. Microfluidics and Nanofluidics, 2013, 14, 767-774.	2.2	17
99	EUV induced ablation and surface modification of poly(vinylidene fluoride) irradiated in vacuum or gaseous environment. Proceedings of SPIE, 2013, , .	0.8	1
100	Simultaneous treatment of polymer surface by EUV radiation and ionized nitrogen. Applied Physics A: Materials Science and Processing, 2012, 109, 39-43.	2.3	52
101	Polyethyleneimine coating renders polycarbonate resistant to organic solvents. Lab on A Chip, 2012, 12, 2580.	6.0	27
102	Preparation of a Responsive Carbohydrate-Coated Biointerface Based on Graphene/Azido-Terminated Tetrathiafulvalene Nanohybrid Material. ACS Applied Materials & Interfaces, 2012, 4, 5386-5393.	8.0	44
103	Hydrophilic polycarbonate for generation of oil in water emulsions in microfluidic devices. Lab on A Chip, 2011, 11, 1151.	6.0	26
104	Hydrophobic modification of polycarbonate for reproducible and stable formation of biocompatible microparticles. Lab on A Chip, 2011, 11, 748-752.	6.0	48
105	Surface and in-depth characterization of InGaN compounds synthesized by plasma-assisted molecular beam epitaxy. Journal of Alloys and Compounds, 2011, 509, 9565-9571.	5.5	14
106	Hydrogen-assisted dechlorination of 1,2-dichloroethane on active carbon supported palladium–copper catalysts. Catalysis Today, 2011, 175, 576-584.	4.4	34
107	Preferential oxidation of CO in H2 rich stream (PROX) over gold catalysts supported on doped ceria: Effect of water and CO2. Catalysis Today, 2011, 175, 411-419.	4.4	33
108	Preparation and characterization of monometallic (Au) and bimetallic (Ag/Au) modified-titania photocatalysts activated by visible light. Applied Catalysis B: Environmental, 2011, 101, 504-514.	20.2	205

#	Article	IF	CITATIONS
109	Gold supported on ceria doped by Me3+ (Me = Al and Sm) for water gas shift reaction: Influence of dopant and preparation method. Catalysis Today, 2010, 158, 69-77.	4.4	20
110	Decomposition of thin titanium deuteride films; thermal desorption kinetics studies combined with microstructure analysis. Applied Surface Science, 2008, 254, 2629-2637.	6.1	12
111	Tem studies of microstructural transformations in thin Iron films induced by vacuum annealing. Microscopy and Microanalysis, 2002, 8, 1438-1439.	0.4	0
112	TEM and SEM studies of microstructural transformations of thin iron films during annealing. Applied Surface Science, 2002, 189, 148-156.	6.1	15
113	Low-temperature interaction of hydrogen with methane-precovered thin palladium films. Surface Science, 1994, 312, 157-166.	1.9	6
114	Kinetics and thermodynamics of hydrogen interaction with thin cobalt films. Applied Surface Science, 1989, 35, 399-408.	6.1	19
115	The kinetics of the low-temperature hydrogen interaction with polycrystalline cobalt films. Applied Surface Science, 1989, 37, 272-282.	6.1	13
116	A Comparative Study of Nanosized Gold and Copper Catalysts on Y-doped Ceria for the Water-Gas Shift Reaction. , 0, , .		0